PCCP

View Online
Dynamic Article Links

Cite this: DOI: 10.1039/c1cp22664a

www.rsc.org/pccp

PAPER

V-doped SnS_2: a new intermediate band material for a better use of the solar spectrum

Perla Wahnón,*[a] José C. Conesa,*[b] Pablo Palacios,[a] Raquel Lucena,[b] Irene Aguilera,[a] Yohanna Seminovski[a] and Fernando Fresno[b]

Received 19th August 2011, Accepted 16th September 2011
DOI: 10.1039/c1cp22664a

Intermediate band materials can boost photovoltaic efficiency through an increase in photocurrent without photovoltage degradation thanks to the use of two sub-bandgap photons to achieve a full electronic transition from the valence band to the conduction band of a semiconductor structure. After having reported in previous works several transition metal-substituted semiconductors as able to achieve the electronic structure needed for this scheme, we propose at present carrying out this substitution in sulfides that have bandgaps of around 2.0 eV and containing octahedrally coordinated cations such as In or Sn. Specifically, the electronic structure of layered SnS_2 with Sn partially substituted by vanadium is examined here with first principles quantum methods and seen to give favourable characteristics in this respect. The synthesis of this material in nanocrystalline powder form is then undertaken and achieved using solvothermal chemical methods. The insertion of vanadium in SnS_2 is found to produce an absorption spectrum in the UV-Vis-NIR range that displays a new sub-bandgap feature in agreement with the quantum calculations. A photocatalytic reaction-based test verifies that this sub-bandgap absorption produces highly mobile electrons and holes in the material that may be used for the solar energy conversion, giving experimental support to the quantum calculations predictions.

I. Introduction

In photovoltaic (PV) technology increasing the efficiency of PV cells is a permanent goal. One possible way of enhancing this efficiency, proposed in recent years, is the use of intermediate-band materials.[1] In these systems (Fig. 1) a relatively narrow band (the intermediate band, IB) is located between two other bands (filled and empty, respectively) akin to the valence and conduction bands (VB and CB) of a semiconductor of bandgap width E_g. This allows an electron from the VB to be promoted to the IB, and from the latter to the CB, upon absorption of photons with energy below E_g, achieving the same total result as with one photon of energy E_g or higher. If selective contacts to the VB and CB are built, a higher current can be obtained without sacrificing the photovoltage corresponding to the full bandgap E_g, thus increasing the overall efficiency. It has been estimated[1] that the use of this type of material could bring about PV efficiencies with an ideal limit as high as 63.1% (if $E_g \approx 2.0$ eV and the IB is optimally placed between the VB and the CB) while that achievable with one normal absorbing semiconductor (with $E_g \approx 1.1$ eV) is 40.7%

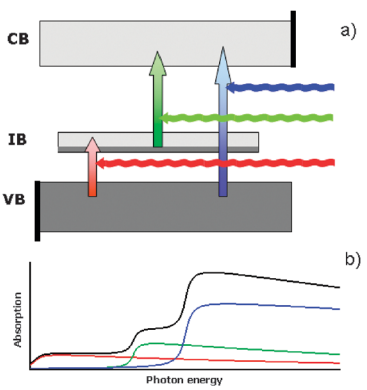

Fig. 1 Intermediate band (IB) working principle: (a) photons of different wavelengths promote electrons from the valence band (VB) directly to the conduction band (CB) and also from the VB to the IB and from the IB to the CB. (b) A wider photon energy range is thus used.

(the Shockley–Queisser limit). Note that this use of two low energy photons to achieve the excitation of one electron across a higher energy gap already operates in natural photosynthesis; the IB concept behaves differently, however, in that both photons are absorbed by the same system, and the direct high energy excitation of an electron through absorption of a shorter wavelength photon is still possible. Note also that this concept could

[a] *Instituto de Energía Solar, Univ. Politécnica de Madrid, Ciudad Universitaria s/n, 28040 Madrid, Spain. E-mail: perla@etsit.upm.es*
[b] *Instituto de Catálisis y Petroleoquímica, CSIC, Marie Curie 2, 28049 Madrid, Spain. E-mail: jcconesa@icp.csic.es*

also improve the efficiency of photocatalytic processes, based on the transfer of photogenerated electrons and holes to molecules adsorbed on surfaces, as a wider range of the light spectrum could be used thanks to the IB.

In this scheme the IB should be partially filled, to allow comparable rates for both low energy photon absorption steps, and should not overlap in energy with the CB nor the VB to avoid a fast transfer to the IB, *via* thermalization, of the carriers excited into the VB and CB. A well-formed band with significant dispersion and delocalization is also needed, rather than discrete localized levels that would favour non-radiative recombination; the minimum dopant concentrations necessary to fulfil this condition when forming the IB *via* doping have been estimated.[2]

Some of the first proposals to carry out the IB concept were based on quantum dots,[3] and although proof-of-concept of the principle could be obtained with them[4] the perspectives of achieving an efficient system on this basis seem slight as the absorbing centers are very diluted leading to rather small absorption coefficients. Thus single phase materials allowing higher concentrations of IB-forming components are preferable. According to this, several doped semiconductors have been proposed to form the appropriate IB materials. O-doped (Zn,Mn)Te and N-doped Ga(As,P) have been claimed, on the basis of spectroscopic data interpreted with a band anticrossing model, to form IB structures,[5,6] although full first-principles quantum calculations were not made on these systems.

On the other hand previous works by the present authors have shown, using Density Functional Theory (DFT) calculations, that IB materials can be obtained if judiciously chosen transition metals are inserted into certain semiconductors. In Si itself this can be achieved with interstitial Ti atoms, and the calculation results[7] agree with experimental data obtained on specimens made by ion implantation of Ti at high doses in Si wafers.[8] The substitutional insertion of significant amounts of S or Se into Si, as achieved recently in the laboratory,[9] can also produce adequate IB materials when coupled with p-doping, according to DFT calculations.[10] However, Si is not the best host material for implementing the IB-PV concept, since its bandgap is not near the optimum one (2.0 eV as said above) that would allow the maximum efficiency to be obtained in an IB PV cell, and therefore these Si-based systems are useful mainly in fundamental studies of the IB principle. Only resorting to metastable Si polymorphs, such as the type II Si clathrates that have $E_g = 1.9$ eV,[11] can silicon lead to an optimum IB material, as seems to be the case, according to our DFT results,[12] when Ag or V are introduced into specific positions of their microporous structures.

Useful IB materials should be easier to obtain starting from semiconductors which, having a bandgap near the optimum, are already being used in PV technology. Thus DFT calculations have shown that an IB appears when a light transition metal (TM) such as Ti or Cr partially substitutes Ga atoms in tetrahedral semiconductors such as GaAs or GaP[13,14] or the chalcopyrite $CuGaS_2$.[15] More recently, DFT calculations of ours have predicted that an IB appears as well in indium containing sulfides of spinel-type structure when part of the octahedral In atoms in them are substituted by Ti or V;[16] realising in practice this latter type of substitution is expected to be easier since octahedral coordination is normally preferred by this type of transition metal. It may be noted here that, although standard DFT calculations have deficiencies in predicting correctly the electronic structures in solids and especially the band gaps, the problem can be solved using advanced quantum methods such as GW theory, as is being proven at present by us for some selected examples of these IB materials.[17] It is worth noting finally that in the case of V-substituted In_2S_3, these theoretical predictions have received subsequent experimental support, proving that indeed IB materials of types amenable to incorporation into practical PV devices can be obtained following this strategy.[18]

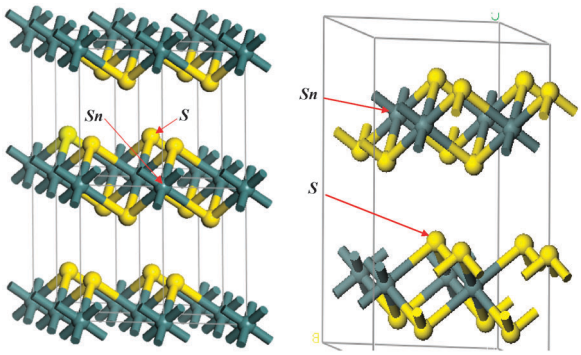

Fig. 2 Crystal structures of SnS_2 polytypes: (left) 2H; (right) 4H, in the 2 × 2 × 1 supercell used in the DFT calculations.

Taking into account the same principle we examine here the possible formation of an IB in SnS_2. This material is a semiconductor having a hexagonal layered crystalline structure in which Sn is octahedrally coordinated. Several polytypes of it exist[19] (see drawings of the most common ones in Fig. 2) due to the possibility of different layer stacking sequences; all of them are known to have very similar band gaps of around 2.2–2.3 eV.[20,21] As will be shown below, theory predicts, and experiments support, that an IB with the desired characteristics can be produced in it through metal atom substitution.

II. Methods

A. Calculations

Our calculations were made using spin-polarized DFT with the generalized gradient (GGA) approximation and the Perdew–Wang 1991 functional.[22] The plane-wave VASP code[23] with PAW potentials[24,25] was used; these left the 5s5p, 3s3p and 4s3d electron shells for Sn, S and V atoms, respectively, in the valence space. The plane-wave cutoff was set as 280 eV, and Brillouin zone sampling was carried out with a Monkhorst-Pack (8 × 8 × 8) grid;[26] both were verified to provide convergence in total lattice energy within 0.001 eV atom^{-1}. Unconstrained relaxations of ions and cells with a convergence tolerance of 0.01 eV Å^{-1} for atomic forces were made for all systems.

From the resulting converged wave functions, total and projected density of states (PDOS), band diagrams and optical properties were computed. For the latter we calculated the real and imaginary parts of the dielectric function, as well as the absorption coefficient.[27,28] We considered only direct transitions. To get well converged electronic properties and the frequency dependent dielectric tensor, a 364 eV energy cutoff for the basis

set and 200 empty bands were used. A 17 × 17 × 17 grid was needed to sample the Brillouin zone.

These calculations were carried out here for the 4H polytype of SnS_2[29] and for a 2 × 2 × 1 supercell of it (Fig. 2) in which 25% of the Sn atoms (one in each layer, *i.e.* two atoms per unit cell) were substituted by V; the unit cell stoichiometry is thus $V_2Sn_6S_{16}$. Similar electronic structures are expected to appear in the different polytypes for one same degree of substitution.

B. Experimental

Materials and synthesis. $SnCl_4{\cdot}5H_2O$ (Aldrich 98%), VCl_4 (Aldrich 99%), thiourea (Aldrich 99%) and Triton X-100 surfactant (Sigma-Aldrich) were used as received. For the synthesis of SnS_2, which is reported elsewhere,[30] $SnCl_4$ (3.83 mmol) and thiourea (9.95 mmol) were dissolved in 85 mL of a mixture of Triton X-100 and deionized water (6 : 94 ratio by volume), and introduced into a 125 cm^3 Teflon-lined stainless steel autoclave. For the synthesis of the V-doped material, not reported previously, the same procedure was followed, except that $SnCl_4{\cdot}5H_2O$ (3.59 mmol) and VCl_4 (0.52 mmol) instead of only $SnCl_4{\cdot}5H_2O$ were used. In all cases the solutions were prepared under nitrogen in a glove bag, and the final pH value was adjusted to 3.0 with HCl (Panreac 35%). The closed autoclave was heated to 453 K in an oven for 48 h, after which it was cooled to ambient temperature and then its content was filtered and the solid powder product (orange-yellow in the case of SnS_2 preparations, greenish in the case of the V-containing material) was washed first 5 times in deionized water and then 3 times in methanol, and finally dried in air at 333 K.

Characterization. Chemical analysis of the materials was carried out with X-ray fluorescence using a Rich & Seifert TXRF EXTRA-II spectrometer. Powder X-ray diffraction diagrams in Bragg–Brentano geometry were obtained with a Philips X'Pert Pro PANalytical diffractometer using Cu Kα radiation. Simulated patterns and pattern fittings were obtained using the PowderCell[31] program. UV-Vis-NIR spectra were obtained in diffuse reflectance mode using a Varian Cary 5000 spectrophotometer and Spectralon® as reference material.

X-band EPR spectra (in the standard form of first derivative of the absorption spectra) were taken at 77 K or ambient temperature in weighted portions of the sample held in a closed and evacuated quartz tube with a Bruker ER 200D instrument interfaced to a digital data acquisition system. The number of EPR-detectable spins was determined from them through double integration and comparison with the result obtained similarly for a weighted portion of standard $CuSO_4{\cdot}5H_2O$ (Aldrich 99,99%), measured at the same temperature. The known dependence between the integrated value and the *g* factor[32] was taken into account.

Photocatalytic tests. The photocatalytic activity for the oxidation of formic acid (1.5 mM) was measured in an aqueous suspension of the sulfide materials. Since both formic acid and the formate ion have no light absorption in the visible and near-UV ranges, and their oxidation products produce equally no light absorption, by using this reactant it is ensured that the results depend exclusively on light absorption in the solid. The water-thermostated pyrex glass reactor, containing 40 mg of sulfide powder in 80 mL of suspension (which was naturally aerated through magnetic stirring under ambient atmosphere), was irradiated from above through a pyrex window using an ozone-free 450 W Xenon lamp from Spectratech provided with a collimating condenser lens, a water filter (to suppress IR components) and one of the collection of band-pass optical filters (Andover Corporation) transmitting a wavelength interval of FWHM width ~50 nm. The intensity of the light incident on the liquid surface could be checked prior to the reaction with a Newport 842-PE radiometer, and was verified to be more or less the same with the different filters in the wavelength range explored. The evolution of reactant was monitored by sampling a small volume (1.5 mL) of the suspension at given time intervals, which was filtered with a nylon 0.45 μm filter to separate the solid, and measuring the formic acid concentration in the liquid with a UV-Vis Shimadzu UV-2100 spectrometer through its absorbance at λ = 205 nm.

III. Results and discussion

A. DFT calculations

For the pure SnS_2 semiconductor, *i.e.* with no TM inserted, the calculation produces a unit cell with dimensions a = 3.69 Å, c = 12.38 Å after full geometry relaxation, slightly above the experimental ones (a = 3.645 Å, c = 11.802 Å);[29] the Sn–S bond length obtained (d = 2.59 Å) is also a bit higher than the experimental value (d = 2.570 Å). These deviations are typical for the GGA approach. The computed density of states is shown in Fig. 3a; the gap obtained (1.37 eV, indirect type) is 0.83 eV lower than the experimental value as is usual in GGA calculations.

For SnS_2 with Sn partially substituted by V the crystal lattice is slightly contracted (a = 3.65 Å, c = 12.26 Å). The mean nearest neighbour V–S distance is 2.43 Å (*i.e.* S atoms approach the V atom more than Sn ones, as expected due to the smaller size of the former); it is however 0.08 Å larger than that existing in VS_2, d = 2.351Å.[33]

Total DOS and PDOS (projecting on the metal 3d orbitals) computed for the V-substituted system are displayed in Fig. 3b. After full geometry relaxation the electronic structure contains strongly spin-polarized levels that come about from the 3d metal states. Both majority and minority spin levels appear to be split into two branches; as shown in Fig. 3c, which displays the obtained band structure diagrams, for both spins the lower branch contains three states per vanadium atom, as expected for TM atoms in a nearly octahedral environment, which will split in each metal the 3d levels in a lower lying triply degenerated t_{2g}-like manifold and an upper lying doubly degenerated e_g-like manifold. For the majority spin states the lower branch is crossed by the Fermi energy so that it contains one electron per vanadium atom (as expected from the $3d^1$ configuration of its tetravalent state), while the upper branch appears inside the CB. For the minority spins both branches are empty, the lower one overlapping the majority spin lower branch but not the conduction band. An intermediate band is therefore clearly formed; its width is relatively large due to the high concentration of V atoms, which leads to extensive 3d orbital overlap and delocalization, but is not large enough that it may overlap the CB or VB.

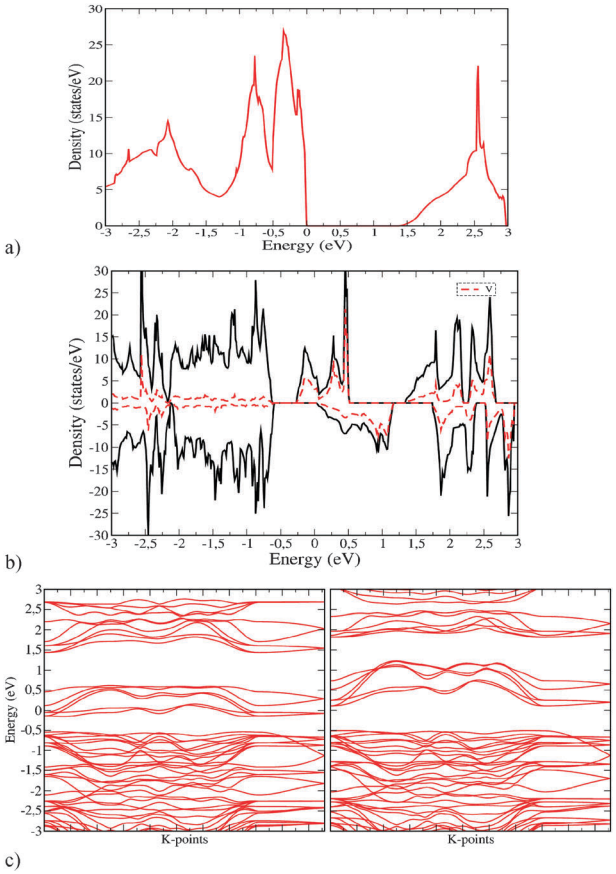

Fig. 3 DFT results: density of states (DOS) computed for (a) undoped SnS_2 and (b) the $V_2Sn_6S_{16}$ structure (for the latter the vanadium 3d orbital projected DOS, PDOS, is shown in dashed line). (c) Band structure computed for $V_2Sn_6S_{16}$, with majority and minority spin curves shown, respectively, on the left and right sides. $E = 0$ marks the Fermi level in all cases.

With these calculations optical properties can be computed. A scissors operator correction to compensate for the gap underestimation typical of GGA was not applied, since it is not clear how the shift should be applied in the case of an IB material, and our aim here is to see what could be the effect of the vanadium insertion on the photon absorption spectrum. Results are displayed in Fig. 4. On side (a) the absorption coefficient obtained for the V-containing material is compared to that obtained for the undoped semiconductor; on side (b) the closely related imaginary part of the dielectric constant is decomposed in the contributions of the different interband transitions. Apart from a component at the lowest energies ($E < 0.7$ eV), due to transitions within the partially filled IB, the transitions between the IB and the CB or VB not only increase significantly the overall absorption coefficient but are also seen to cover a substantial range of sub-bandgap photon energies, which undoped SnS_2 cannot absorb, making thus possible, in principle, the photovoltaic use of a wider range of the sunlight spectrum.

B. Experimental results

Characterization of materials. As reported elsewhere[30] the undoped polycrystalline tin sulfide material obtained hydrothermally displays a powder X-ray diffractogram (XRD)

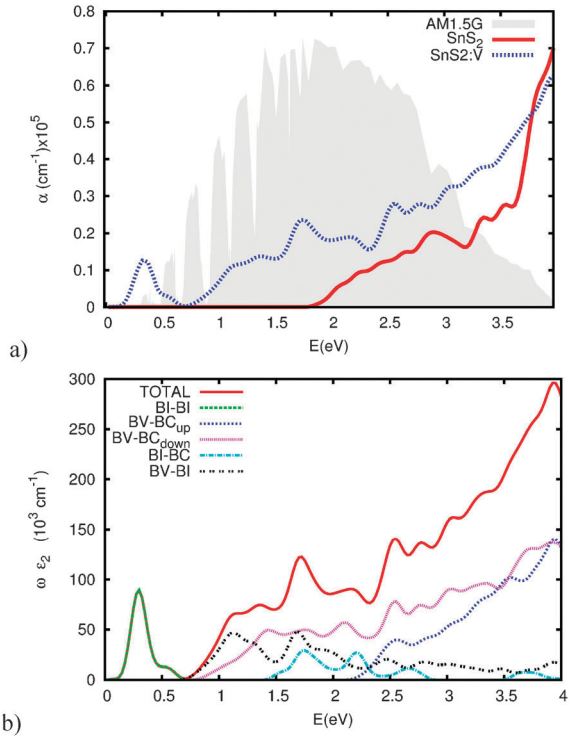

Fig. 4 Optical properties computed with DFT: (a) absorption coefficient computed for both SnS_2 and $V_2Sn_6S_{16}$ structures, compared with the standard AM1.5 sunlight spectrum in the shadowed plot. (b) Contributions, in the $V_2Sn_6S_{16}$ case, of the different inter- or intraband transitions to the imaginary component of the dielectric constant.

(Fig. 5a) in good agreement with the 2H polymorph[34] of SnS_2 (JCPDS 23-0677 pattern). Peak fitting gives cell parameters $a = 3.649$ Å, $c = 5.899$ Å in reasonable agreement with experimental values ($a = 3.645$ Å, 5.891 Å);[19] a crystallite size of $d \approx 23$ nm can be obtained from the peak widths by applying the Scherrer formula. Its diffuse reflectance (DR) UV-Visible-near IR spectrum (Fig. 5b) also agrees with the reported bandgap of this material; a weak sub-bandgap absorption tail is observed which may be due to surface states or defects producing in-gap levels located near the band edges (Urbach tail). The reaction leading to this product can be written as

$$SnCl_4 + 2\,(NH_2)_2CS + 4\,H_2O \rightarrow SnS_2 + 4\,NH_4Cl + 2\,CO_2 \quad (1)$$

The V-containing specimen prepared by the hydrothermal method had a V : Sn : S atomic ratio of 0.155 : 0.83 : 2.0 according to the XRF chemical analysis. Its XRD diagram, also presented in Fig. 5a, reveals again a well-crystallized material having the same diffraction peaks as undoped SnS_2; no additional feature indicating the presence of vanadium-related phases or amorphous components was found, suggesting the formation of a solid solution. The crystallite size deduced from the XRD linewidth is $d \approx 30$ nm, while the cell parameters obtained through pattern fitting are $a = 3.645$ Å, $c = 5.8995$ Å. The decrease in parameter a upon introduction of V is lower than that predicted taking into account the DFT data; but these are obtained for a structure in which V atoms are regularly ordered within a supercell, while in the real

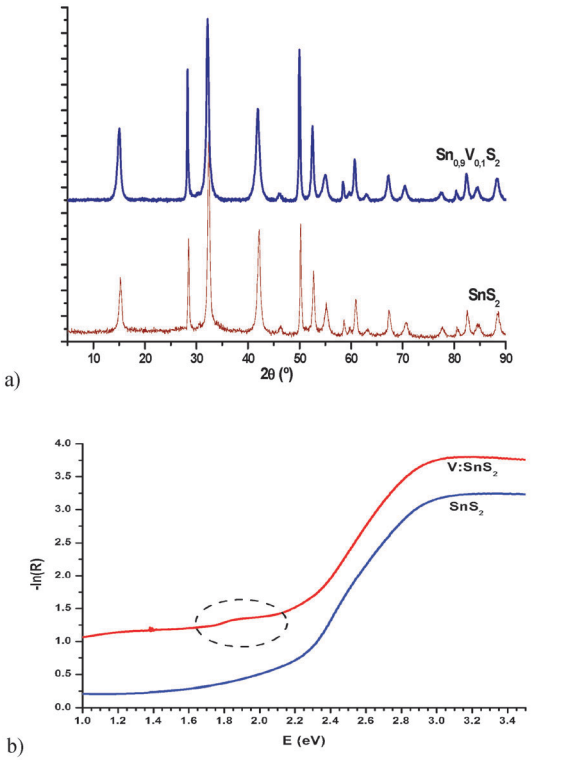

Fig. 5 Characterization of the sulfide materials made: (a) XRD diagrams; (b) diffuse reflectance UV-Vis-NIR spectra.

situation their location will be random, so that it is uncertain whether a decrease equal to the predicted one should be expected.

The UV-Vis-NIR spectrum of this V-containing material is also displayed in Fig. 5b. A new absorption feature is seen to appear in the range below 2.2 eV, with a distinct edge at *ca.* 1.6 eV and superimposed on the Urbach tail, indicating a new, distinct channel for the absorption of photons having energies clearly below the bandgap of SnS_2. This is rather similar to the new feature appearing in the theoretically computed spectrum shown in Fig. 4a. Note that, while the exact positions of the absorption onsets cannot be predicted by standard DFT as said above, the prediction of the shift in such onset that occurs upon V introduction can be considered to be more reliable.

To check the state of vanadium in this specimen EPR spectra were taken on it at both ambient temperature and 77 K; they are presented in Fig. 6. A signal centered at $g = 1.968$ was found, ascribable to V^{4+} centers. This averaged g value is intermediate between that found for octahedral V^{4+} molecular complexes having all-sulfur and all-oxygen ligands,[35] but since these values depend significantly on the solvent or the matrix a clear idea of the nature of the vanadium first neighbours cannot be obtained. The relatively large signal linewidth ($\Delta H_{pp} \approx 225$ Gauss) is probably due to mutual magnetic interactions between the V^{4+} ions in the concentrated sample. The spectra at both temperatures are similar except for the intensity, which follows rather well the T^{-1} behaviour typical of normal paramagnetic species. Particularly relevant, besides the observation of this normal paramagnetic behaviour (which excludes the presence of significant exchange interactions between the V^{4+} ions, as would

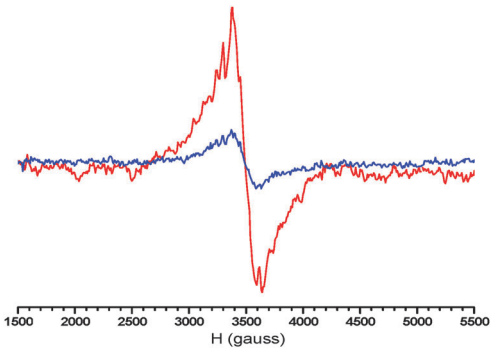

Fig. 6 EPR spectra at ambient temperature (small signal) and 77 K (large signal) of the V-doped SnS_2 specimen.

probably occur if direct V–S–V or V–O–V links were present), is the fact that the integrated intensity, once compared with the $CuSO_4$ standard, accounts for *ca.* 90–95% of all the V atoms present. Both observations indicate that practically all of the substituting element is in the V^{4+} state, as expected, and in a relatively dilute state, supporting, together with the absence of new features in the XRD diagram, the assumption that these ions are integrated in the SnS_2 matrix forming a solid solution. Some narrower peaks observed with low intensity can also be ascribed to a minor amount of isolated V^{4+} ions, their splitting being due to hyperfine interaction with the magnetic moment of the V nucleus.

Photoactivity spectral response. The ability to form electrons and holes under irradiation which are able to be used in a practical way can be checked without building a photovoltaic or electrochemical device by examining the photocatalytic properties of the material in powder form. In photocatalysis, electrons and holes are photogenerated in a semiconductor which is in contact with a gas or liquid, and if they are able to move easily through the CB and VB they diffuse to its surface where they are transferred to molecules in the fluid leading to chemical reactions the products of which can be detected. The ability to carry out a photocatalytic redox reaction can be thus correlated directly with the photovoltaic capabilities of the material. Here the strategy followed consists of checking the photocatalytic properties of the synthesized materials when irradiated in an aqueous suspension containing O_2 and a simple organic molecule, formic acid. The electron transfer processes that would occur on the solid surface would lead to the simple overall oxidation reaction

$$HCOOH + 1/2\ O_2 \rightarrow CO_2 + H_2O \qquad (2)$$

and can be followed by examining the formic acid concentration decrease under irradiation with light of different wavelengths.

This process was already checked for the undoped SnS_2 in a previous work,[30] where it was found that the initial rate of HCOOH degradation after start of irradiation depends on the incident light wavelength with a similar pattern as the SnS_2 light absorption coefficient. The same test was carried out now for the V-containing sample; the observed HCOOH concentration decay for different light wavelengths is shown in Fig. 7, where it is compared with the results previously obtained on the SnS_2 sample. In these latter, the small photocatalytic activity

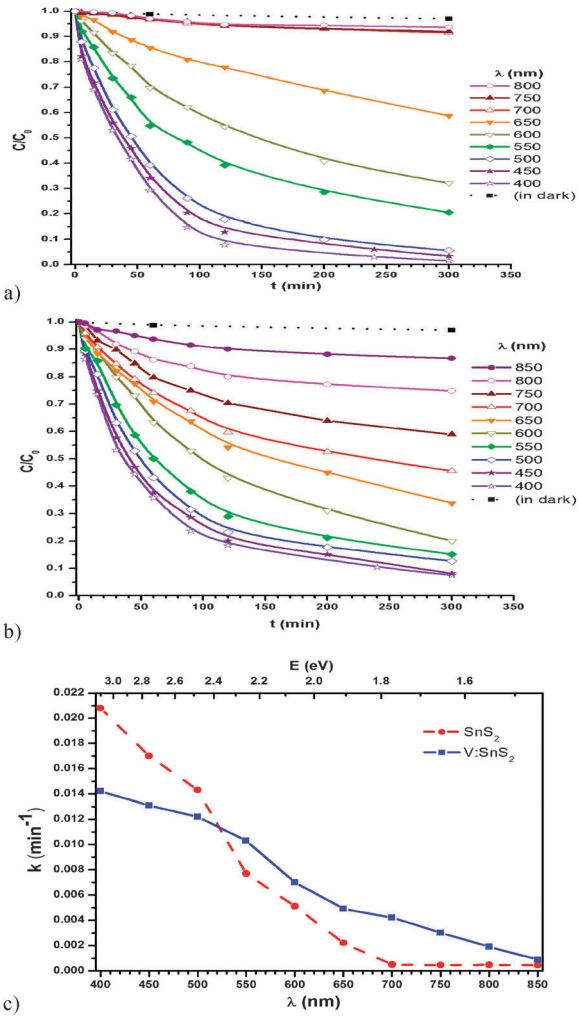

Fig. 7 Upper curves: HCOOH degradation by irradiation with light of different wavelengths in aqueous suspension with SnS_2 (a) and V : SnS_2 (b). Lower curves (c): rate constant for these processes plotted as a function of light wavelength.

observed with filters of nominal wavelengths up to 650 nm (higher than the 565 nm value corresponding to the SnS_2 gap) can be explained as due to the combination of the Urbach tail absorption and the width of the spectral band transmitted by the filters.

For photons with energy higher than the SnS_2 gap width the photocatalytic efficiency of the V-containing sample appears lower than that of pure SnS_2, which may be due to some recombination induced by defects or by isolated V centers at the bulk or the surface; but for a range of wavelengths above the 650 nm limit in which pure SnS_2 is unable to use photons for the process the V-containing sample produces a significantly larger reaction rate. This is seen also clearly in Fig. 7, which plots the value of the effective reaction rate constant k, measured for both samples from the slope at $t = 0$ of a semilogarithmic plot (not shown), as a function of the light wavelength. This correlates with the presence of a new sub-bandgap photon absorption feature observed in Fig. 5b, and confirms that the insertion of the intermediate band predicted by the DFT calculations contributes to generating electrons and holes, which may occur thorough the absorption of two sub-bandgap photons as in the model explained above.

IV. Conclusions

The present work shows that an intermediate band of the type that may enhance photovoltaic solar efficiency can appear through the simple partial substitution of Sn by V in the octahedral semiconductor SnS_2. As shown here this system, which includes only elements relatively abundant in nature, can be synthesized in powder form with a hydrothermal method, and both its modified absorption coefficient and its photocatalytic behaviour agree with the DFT prediction, showing an extension of the active spectral range beyond the SnS_2 bandgap edge even in this non-optimized preparation.

By itself, this latter result is relevant for the applications of photocatalysis, a chemical process which has not only been intensely studied and applied for pollution abatement processes in the last decades,[36] but is being tried nowadays as well for energy-oriented uses like the splitting of water into H_2 and O_2,[37] the capture of CO_2 to produce organic molecules[38] (note that these processes would constitute two forms of artificial photosynthesis) or the low temperature reforming of biomass or biofuels to give H_2 (an energy-saving way of using renewable resources).[39] But the result also allows us to expect that, if the material presented here can be made in thin film form with any of the existing technologies, and is then engineered into a photovoltaic device with the proper contacting layers, a significant enhancement in the efficiency of photovoltaic solar cells can be obtained, fulfilling the expectations of the IB PV cell proposal.

Acknowledgements

This work was carried out with support from projects GENESIS-FV of the Consolider-Ingenio programme (project nr. CSD2006-0004) and FOTOMAT of the Plan Nacional de Materiales (project nr. MAT2009-14625-C03), both financed by the Spanish Plan Nacional de Investigación, and programme NUMANCIA-2 (code nr. S2009ENE-1477) financed by the Comunidad de Madrid. R. L. thanks also the CSIC for a PhD grant of its I3P programme, under which this research was undertaken. Y. S. thanks the MICINN for the PhD grant. Authors thankfully acknowledge the computer resources, technical expertise and assistance provided by the Centro de Supercomputación y Visualización de Madrid (CeSViMa) and the Spanish Supercomputing Network.

References

1 A. Luque and A. Martí, *Phys. Rev. Lett.*, 1997, **78**, 5014.
2 A. Luque, A. Martí, E. Antolín and C. Tablero, *Physica B (Amsterdam)*, 2006, **382**, 320.
3 See *e. g.* P. G. Linares, A. Martí, E. Antolín and A. Luque, *J. Appl. Phys.*, 2011, **109**, 014313, and references therein.
4 E. Antolín, A. Martí, C. R. Stanley, C. D. Farmer, E. Cánovas, N. López, P. G. Linares and A. Luque, *Thin Solid Films*, 2008, **516**, 6919.
5 K. M. Yu, W. Walukiewicz, W. Shan, J. Wu, J. W. Beeman, M. A. Scarpulla, O. D. Dubon and P. Becla, *J. Appl. Phys.*, 2004, **95**, 6232; K. M. Yu, W. Walukiewicz, J. W. Ager, D. Bour, R. Farshchi, O. D. Dubon, S. X. Li, I. D. Sharp and E. E. Haller, *Appl. Phys. Lett.*,

2006, **88**, 092110; N. Lopez, L. A. Reichertz, K. M. Yu, K. Campman and W. Walukiewicz, *Phys. Rev. Lett.*, 2011, **106**, 028701.
6 W. M. Wang, A. S. Lin and J. D. Phillips, *Appl. Phys. Lett.*, 2009, **95**, 011103.
7 K. Sánchez, I. Aguilera, P. Palacios and P. Wahnón, *Phys. Rev. B: Condens. Matter*, 2009, **79**, 165203.
8 G. González-Díaz, J. Olea, I. Mártil, D. Pastor, A. Martí, E. Antolín and A. Luque, *Solar Energy Mater. Solar Cells*, 2009, **93**, 1668.
9 B. P. Bob, A. Kohno, S. Charnvanichborikarn, J. M. Warrender, I. Umezu, M. Tabbal, J. S. Williams and M. J. Aziz, *J. Appl. Phys.*, 2010, **107**, 123506.
10 K. Sánchez, I. Aguilera, P. Palacios and P. Wahnón, *Phys. Rev. B: Condens. Matter*, 2010, **82**, 165201.
11 J. Gryko, P. F. McMillan, R. F. Marzke, G. K. Ramachandran, D. Patton, S. K. Deb and O. F. Sankey, *Phys. Rev. B: Condens. Matter*, 2000, **62**, R7707.
12 P. Palacios, J. C. Conesa and P. Wahnón, submitted.
13 P. Wahnón and C. Tablero, *Phys. Rev. B: Condens. Matter*, 2002, **65**, 165115; C. Tablero and P. Wahnón, *Appl. Phys. Lett.*, 2003, **82**, 151.
14 P. Wahnón, P. Palacios, J. J. Fernández and C. Tablero, *J. Mater. Sci.*, 2005, **40**, 1383; P. Palacios, J. J. Fernández, K. Sánchez, J. C. Conesa and P. Wahnón, *Phys. Rev. B: Condens. Matter*, 2007, **73**, 085206.
15 P. Palacios, K. Sánchez, J. C. Conesa and P. Wahnón, *Phys. Status Solidi A*, 2006, **203**, 1395; P. Palacios, K. Sánchez, J. C. Conesa, J. J. Fernández and P. Wahnón, *Thin Solid Films*, 2007, **515**, 6280.
16 P. Palacios, I. Aguilera, K. Sánchez, J. C. Conesa and P. Wahnón, *Phys. Rev. Lett.*, 2008, **101**, 046403.
17 I. Aguilera, P. Palacios and P. Wahnón, *Phys. Rev. B: Condens. Matter*, 2011, **84**, 115106.
18 R. Lucena, I. Aguilera, P. Palacios, P. Wahnón and J. C. Conesa, *Chem. Mater.*, 2008, **20**, 5125.
19 R. S. Mitchell, Y. Fujiki and Y. Ishizawa, *Nature*, 1974, **247**, 537.
20 D. L. Greenaway and R. Nitsche, *J. Phys. Chem. Solids*, 1965, **26**, 1445.
21 M. J. Powell, E. A. Marseglia and W. Y. Liang, *J. Phys. C: Solid State Phys.*, 1978, **11**, 895; R. Bacewicz, B. Palosz, W. Palosz and S. Gierlotka, *Solid State Commun.*, 1985, **54**, 283.
22 J. Perdew, J. A. Chevary, S. H. Vosko, K. A. Jackson, M. R. Pederson, D. J. Singh and C. Fiolhais, *Phys. Rev. B: Condens. Matter*, 1992, **46**, 6671.
23 G. Kresse and J. Hafner, *Phys. Rev. B: Condens. Matter*, 1993, **47**, R558.
24 G. Kresse and D. Joubert, *Phys. Rev. B: Condens. Matter*, 1999, **59**, 1758. All PAW potentials used, from the VASP library, are obtained by the method explained in this reference.
25 P. E. Blöchl, *Phys. Rev. B: Condens. Matter*, 1994, **50**, 17953.
26 H. J. Monkhorst and J. D. Pack, *Phys. Rev. B: Condens. Matter*, 1976, **13**, 5188.
27 B. Adolph, J. Furthmüller and F. Bechstedt, *Phys. Rev. B: Condens. Matter*, 2001, **63**, 125108.
28 M. Gajdoš, K. Hummer, G. Kresse, J. Furthmüller and F. Bechstedt, *Phys. Rev. B: Condens. Matter*, 2006, **73**, 045112.
29 J. R. Günter and H. R. Oswald, *Naturwiss. Wochenschr.*, 1968, **55**, 177.
30 R. Lucena, F. Fresno and J. C. Conesa, submitted.
31 Powdercell program, v 2.4, http://www.bam.de/de/service/publikationen/powder_cell.htm
32 R. Aasa and T. Vangard, *J. Magn. Reson.*, 1975, **19**, 308.
33 G. A. Wiegers, *Physica B + C*, 1980, **99**, 151.
34 F. A. S. Al-Alamy, A. A. Balchin and M. White, *J. Mater. Sci.*, 1977, **12**, 2037.
35 See *e. g.* A. Davison, N. Edelstein, R. H. Holm and A. H. Maki, *Inorg. Chem.*, 1965, **4**, 55.
36 J. Blanco-Gálvez, P. Fernández-Ibáñez and S. Malato-Rodríguez, *J. Sol. Energy Eng.*, 2007, **129**, 4.
37 See *e. g.* A. Kudo, *Int. J. Hydrogen Energy*, 2006, **31**, 197; A. L. Stroyuk, A. I. Kryukov, S. Ya. Kuchmii and V. D. Pokhodenko, *Theor. Exp. Chem.*, 2009, **45**, 209.
38 Y. Amao, *ChemCatChem*, 2011, **3**, 458.
39 See *e. g.* T. Montini, V. Gombac, L. Sordelli, J. J. Delgado, X. Chen, G. Adami and P. Fornasiero, *ChemCatChem*, 2011, **3**, 574 and references therein.